

Mechanics of Topologically Interlocked Material Systems under Point Load: Archimedean and Laves Tiling

Andrew Williams, Thomas Siegmund

School of Mechanical Engineering, Purdue University, West Lafayette, IN 47907, USA

Abstract

Topologically interlocked material systems are two-dimensional assemblies of unit elements from which no element can be removed from the assembly without disassembly of the entire system. Consequently, such tile assemblies are able to carry transverse mechanical loads. Archimedean and Laves tilings are investigated as templates for the material system architecture. It is demonstrated under point loads that the architecture significantly affects the force-deflection response. Stiffness, load carrying capacity and toughness varied by a factor of at least three from the system with the poorest performance to the system with the best performance. Across all architectures stiffness, strength and toughness are found to be strongly and linearly correlated. Architecture characterizing parameters and their relationship to the mechanical behavior are investigated. It is shown that the measure of the smallest tile area in an assembly provides the best predictor of mechanical behavior. With small tiles present in the assembly the contact force network structure is well developed and the internal load path is channeled through these stiffest components of the assembly.

Keywords: Architected Material Systems, Plates, Cross-property Relationships, Architecture-Property Relationships

1. Introduction

Plates are ubiquitous two-dimensional structural units able to carry transverse loads. Commonly, plates are monolithic [1], but plates-type structures can also be assembled from topologically interlocked unit elements in the form of convex polyhedra. Planar assemblies of convex polyhedra were considered as early as in the 17th century [2]. A renewed interest in such structures

Preprint submitted to International Journal of Mechanical Sciences

July 17, 2020

7 occurred recently in the civil engineering [3, 4, 5, 6, 7, 8, 9] and materials
8 engineering context [10, 11, 12, 13, 14, 15, 16].

9 In such assemblies individual building blocks (or tiles) are shaped and
10 arranged in the assembly such that no building block can be removed with-
11 out the disassembly of the overall system. When considering such systems
12 in the context of material design [17, 18, 19] they provide a unique method
13 to expand the material property space and for quasi-static loading has been
14 demonstrated to enable the transformation of a brittle response of a mono-
15 lithic plate made of brittle materials (such as ceramics, glasses or brittle
16 polymers) into a quasi-ductile response in the assembled plate-type struc-
17 ture [20, 21, 22]. Moreover, [23] demonstrated that for certain classes of
18 solid-architecture combination a simultaneous improvement of strength and
19 toughness of the assembled plate relative to the monolithic plate is possible.
20 Such favourable mechanical performance of the assembled plate structures
21 also were found to extend to impact loading by altering the relationship be-
22 tween impact velocity and residual velocity [24] and increased impact energy
23 absorption capacity [25, 26, 27]. In addition, assembled plate structures can
24 serve as the template for the implementation of adaptive structural configu-
25 rations [28, 29] to control system stiffness, strength and toughness.

26 In such prior work interlocked assemblies of building blocks have com-
27 monly been considered from the viewpoint of assemblies of all identical build-
28 ing blocks [30]. Such a viewpoint is limiting on what types of architectures
29 can be obtained. The material architecture can be expanded when the start-
30 ing point for the construction of the interlocked material system is an under-
31 lying grid instead of the particles [31, 32, 33, 34, 35, 36]. The construction
32 of topologically interlocked material systems emerging from underlying grid
33 systems is best placed into the context of the theory of tessellations [37] as
34 such an approach provides ordering principles for the architectures of con-
35 cern. The rules set forth in [38] are then applicable to realize the interlocking
36 building blocks related to a tessellation pattern.

37 The present study is connected to a background of prior work on the
38 mechanics of plate-type topologically interlocked assemblies. Prior work on
39 the mechanics of flat vaults [39, 40, 41, 42] has focused on the stability of
40 such systems under gravity loads while a second body of work has considered
41 applied displacement loads [43, 44, 45, 23, 46]. What has emerged is that
42 an understanding of the load-deformation response plate-type topologically
43 interlocked assemblies clearly cannot be conducted within the framework of
44 monolithic plates, and that the assembly architecture shall be an integral

45 part of the description of the respective mechanical response.

46 There has been an absence of systematic investigations into the me-
47 chanical behavior of architected plate systems constructed on the basis
48 of underlying grid systems (tessellations). In prior studies of such system
49 [31, 32, 33, 34, 35, 36] no systematic analysis of the mechanical response of
50 possible architectures even within a confined geometric space has been re-
51 ported. There is furthermore a lack of understanding of the relationships
52 between the system architecture and the mechanical response. This study
53 seeks to fill this gap with the ultimate objective to determine how the me-
54 chanical response of architected plates relates to the underlying tessella-
55 tion patterns. All possible Archimedean and Laves tilings are investigated.
56 Cross-property relationships between stiffness, strength and toughness [47]
57 are determined as relationships between the plate architecture and the plate
58 mechanical response characteristics.

59 2. Methods

60 2.1. Interlocking Assemblies

61 The midplane cross section of a topologically interlocked material (TIM)
62 system is a 2D tiling, and this tiling is considered as the basis for the cre-
63 ation of the TIM system [38]. TIM assemblies are considered as assemblies
64 of blocks (polyhedra) which have center sections conforming to the tilings.
65 Building blocks are constructed from the tiles of the tessellation by first pro-
66 jecting planes from each edge of the tile at alternating angles θ from the
67 normal. In the following the construction principle is reviewed. Without loss
68 in generality the principles are depicted for a square tiling. Code for the
69 generation of the respective geometries is available [48].

70 The magnitude of the edge projection angle θ is a fixed value, but its
71 direction will alternate between angling toward the tile center and away from
72 the tile center for each edge. The projection angle for all configurations in
73 this study was $\theta = 17^\circ$. Within an assembly, the blocks must be oriented such
74 that their edge projection angles are complimentary; if the edge of one tile
75 is angled toward the tile center, the abutting edge of the adjacent tile must
76 be angled away from its center. Once the projection angles are specified,
77 the vertices of the block can be determined. Each block formed from an n -
78 sided tile will have n vertices, and if the tile is a regular polygon, a uniform
79 antiprism block will be formed. Blocks constructed from tiles of different sizes
80 and shapes naturally have differing overall dimensions. In order to control

81 the aspect ratios of the TIM systems it is necessary to truncate the polyhedra
82 to possess a common top and bottom plane in an assembly. Two additional
83 planes must be defined parallel, at distance H_0 and equidistant from the
84 tiling plane. Each building block (i.e. the truncated polyhedra) formed from
85 an n -sided tile now possesses $2n$ vertices. Every set of planes projecting from
86 two consecutive tile edges will yield two vertices, one by computing their
87 intersections with the top plane, Fig. 1(a-b), and the other by computing their
88 intersection with the bottom plane, Fig. 1(c-d). Computing the intersection
89 of all sets of planes projecting from two consecutive edges and the top or
90 bottom planes will locate all the vertices of the block, Fig. 1(e). Edges are
91 then drawn between the vertices to construct the block, Fig. 1(f). In the
92 interlocking assembly, Fig. 1(g), neighboring blocks impose constraints on
93 each other such that assembly is load carrying.

94 2.2. Tile Spaces

95 The Archimedean and the Laves tilings are considered [37]. These tile sets
96 are duals to each other. Archimedean tilings consist of regular polygons only
97 and possess one type of vertex. Laves tilings are defined as having an equal

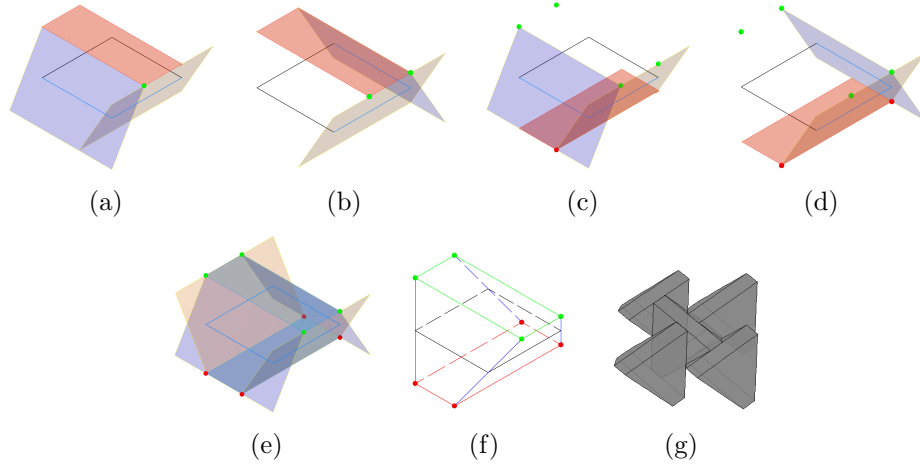


Figure 1: Truncated block construction from a square tile. (a) The intersection of two edge planes and the top plane defines the first top vertex. (b) The intersection of the next two edge planes and the top plane defines the second top vertex. (c) The intersection of two edge planes and the bottom plane defines the first bottom vertex. (d) The intersection of the next two edge planes and the bottom plane defines the next bottom vertex. (e) All planes and all vertices. (f) Wire frame of the resulting block. (g) Assembly of building blocks.

angular spacing of all edges at any vertex [37]. There are 11 Archimedean and 11 Laves tilings. Their structure is described by the naming convention of [37]. Integer numbers with exponents separated by periods and contained within parenthesis describe the common vertex at all tile intersections such that each integer represents the number of sides of a tile that shares the vertex, and the exponent is the number of that type of tile that shares the vertex.

The Archimedean tilings are shown in Fig. 2(a). In a TIM system, the sides of each block must alternate between sloping toward and away from the normal to the plane of tessellation. Therefore, all tiles are required to possess an even number of sides. This restriction eliminates the (3^6) , $(3^4.6)$, $(3^3.4^2)$, $(3^2.4.3.4)$, $(3.4.6.4)$, $(3.6.3.6)$, and (3.12^2) tilings for consideration as a TIM system. The remaining tilings from which TIM systems can be constructed are (4^4) , (6^3) , $(4.6.12)$, and (4.8^2) .

The Laves tilings are shown in Fig. 2(b). Again, TIM systems can only be constructed from a subset of the Laves tilings. The necessity for tiles with an even number of sides when constructing a TIM system eliminates the $[3^4.6]$, $[3^3.4^2]$, $[3^2.4.3.4]$, $[3.12^2]$, $[4.6.12]$, $[4.8^2]$, and $[6^3]$ tilings. The remaining tilings are the $[3^6]$, $[3.6.3.6]$, $[3.4.6.4]$, and $[4^4]$ tilings. The $[4^4]$ and $[3^6]$ tilings are regular tilings and are equivalent to the (4^4) and (6^3) regular Archimedean tilings. Therefore, only the $[3.6.3.6]$ and $[3.4.6.4]$ tilings are added beyond those from the Archimedean tilings.

In summary, the tilings suitable to TIM system construction are the (4^4) (or $[4^4]$), $[3.6.3.6]$, $[3.4.6.4]$, (6^3) (or $[3^6]$), (4.8^2) , and $(4.6.12)$ tilings. The Laves notation was chosen to denote the $[4^4]$ and $[3^6]$ tilings instead of the Archimedean notation of (4^4) and (6^3) because these tilings are more similar to the other Laves tilings than to the other Archimedean tilings in this study. The $[4^4]$, $[3.6.3.6]$, $[3.4.6.4]$, and $[3^6]$ tilings each consist of a single tile, whereas the (4.8^2) tiling consists of two different tiles and the $(4.6.12)$ tiling consists of three different tiles.

By their definition, tilings expand infinitely within a plane, yet here finite size assemblies are considered. Boundaries in the form of a regular polygon are defined for each tiling, such that the tiling was radially symmetric about its center point within the boundary. Squares or hexagons meet this criteria depending on the tiling but it is generally not possible to draw such a boundary without crossing any of the tiles. In such cases, any tiles that were intersected by the border became part of the border. Furthermore, there are multiple possible center points for each tiling, such as centering the bor-

der around different vertices or around the centroid of different tiles. These various boundaries are referred to as A, B, and C variants of a given tiling.

Table 1: Number of tiles and edges lengths for the set of bounded tilings in this work.

Tiling	Tiles	Edge 1 [mm]	Edge 2 [mm]
$[4^4]$ -A	49	29.7	-
$[4^4]$ -B	64	26.0	-
$[3.6.3.6]$ -A	42	30.0	-
$[3.6.3.6]$ -B	46	30.0	-
$[3.4.6.4]$ -A	48	20.0	34.6
$[3.4.6.4]$ -B	48	20.0	34.6
$[3.4.6.4]$ -C	64	17.3	30.0
$[3^6]$ -A	55	15.0	-
$[3^6]$ -B	57	15.0	-
(4.8^2) -A	49	12.2	-
(4.8^2) -B	49	12.2	-
$(4.6.12)$ -A	61	12.7	-
$(4.6.12)$ -B	43	14.6	-
$(4.6.12)$ -C	61	12.6	-

All tilings were made into plate equivalent structures of fixed thickness value and aspect ratio. The thickness of all assemblies was set to $H_0=10.0$ mm. Square and hexagonal shaped assemblies are identical in that L_0 is the radius of the circle inscribed into the square or hexagon, Fig. 2(c). Prior work [43] has shown that a minimum of 7 unit blocks per edge of the assembly is required to create TIM systems suitable for investigation. The value of the in-plane dimension L_0 was derived for the geometric constraints imposed by the $(4.6.12)$ -C assembly. This assembly, by nature of the combination of large and small building blocks imposes an upper limit on L_0 . Geometric constraints for the $(4.6.12)$ -C assembly with 61 blocks lead to an assembly having the ratio $L_0/H_0 = 10.39$. This value of L_0/H_0 is then imposed on all other assemblies. In addition, the condition of 10% truncation of the smallest building block type in an assembly was desired to maintain flat top and bottom planes.

Ideally, all tilings would be constructed to have the same number of block in each assembly. However, the tiling structure imposes geometric constraints that such a condition cannot be met within a fixed L_0/H_0 value and the

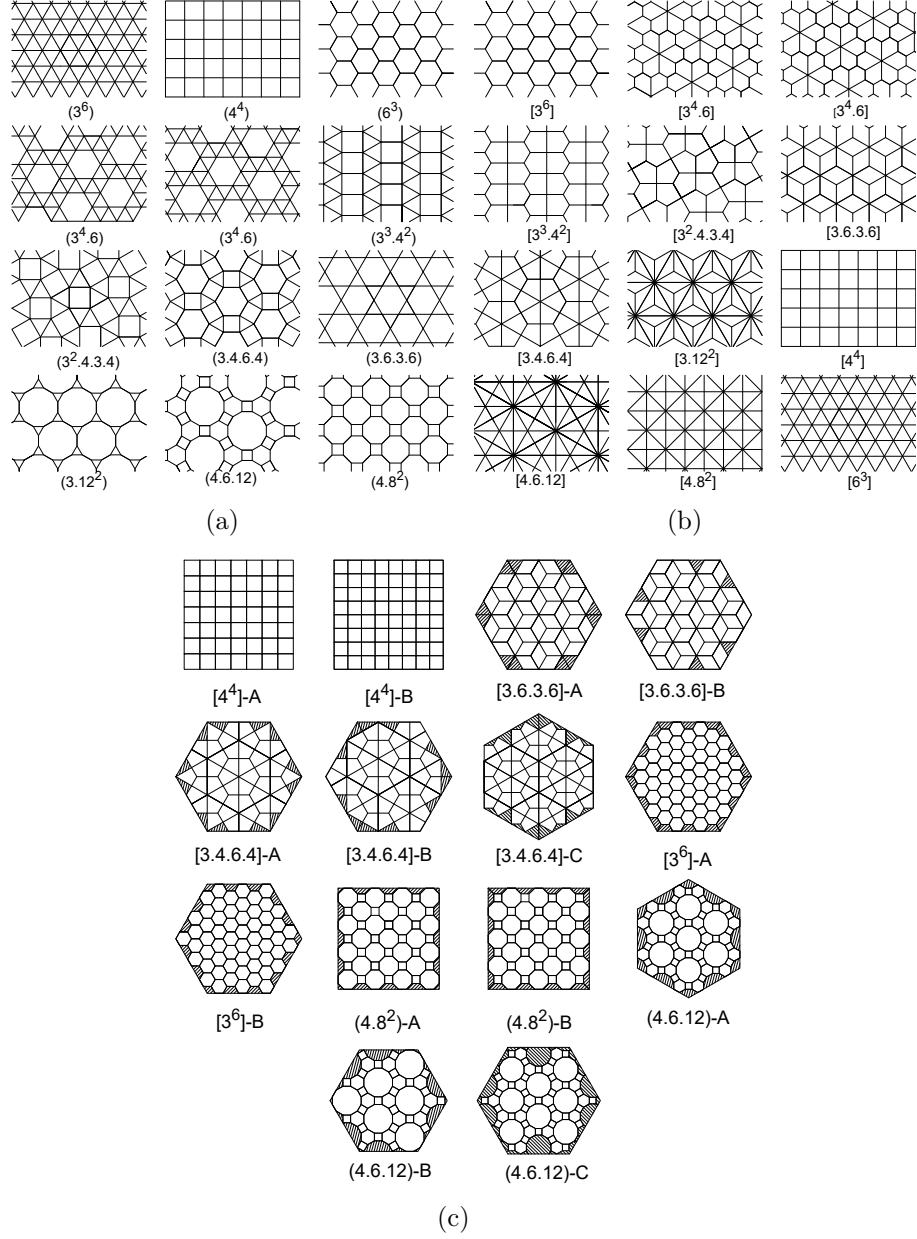


Figure 2: (a) The 11 distinct Archimedean tilings. The $(3^4.6)$ tiling occurs in two forms, both are shown here. (b) The 11 distinct Laves tilings. The $[3^4.6]$ tiling occurs in left-handed and right-handed forms, both are shown here. (c) The set of bounded tilings considered in this work.

155 resulting bounded tilings range from 42 tiles up to 64 tiles, Table 1 and
 156 Fig. 2(c). Table 1 lists all tile edge lengths values. The [3.4.6.4] tiling is the
 157 only tiling considered in this study possessing than one edge length value.

158 TIM systems require a bounding frame (fence) for constraint. The bound-
 159 ing frames were constructed by expanding each tiling beyond the boundaries
 160 drawn in Fig. 2(c) such that there exists a tile adjacent to every side of the
 161 outer tiles in the bounded set. Blocks were generated on these additional
 162 tiles such that the blocks formed from the bounded tiling were completely
 163 surrounded by this additional set of blocks. The blocks in the outermost set
 164 were fused into a single part to serve as a frame for the assembly. The outer
 165 profile of this conglomerate frame was cut into either a square or hexagon
 166 shape as appropriate.

167 The geometry of the single-tile systems is such that they can be flipped
 168 over and rotated to exactly overlay their original position. However, the
 169 multi-tile systems do not typically share this property. The TIM system
 170 configurations used in this study are named after the bounded tiling from
 171 which they were created, and if the response of the assembly is direction
 172 dependent, the load direction will be indicated. For example, the $[4^4]$ -A
 173 assembly is not direction dependent, but the $[4.8^2]$ -A assembly is, therefore
 174 it will be denoted as two separate configurations $[4.8^2]$ -A(-) and $[4.8^2]$ -A(+).
 175 The complete set of TIM system configurations in this study is shown in
 176 Appendix A.

177 2.3. Analysis

178 Finite element models are created for the analysis of the transverse force-
 179 deflection response. Individual building blocks are linear elastic and interact
 180 with each other by contact and friction. Details of the analysis approach are
 181 provided in Appendix B. The analysis approach followed in this study has
 182 been validated in prior work [24]. The bounding frame is considered as rigid.
 183 Displacement boundary conditions are applied such that the bounding frame
 184 is fixed in space. A monotonically increasing displacement (u) transversely to
 185 the assembly plane is imposed onto a rigid indenter. The indenter is located
 186 centrally to the assembly and interacts with the assembly by contact. The
 187 reaction force (F) at the reference node for the indenter is recorded. The
 188 computed force (F)-deflection (u) response is depicted as both raw and
 189 filtered data. The total work ALLWK, the strain energy ALLSE and friction
 190 dissipation ALLFD are computed in dependence of the applied displacement.

System characteristic points are marked on the F - u plots and these were extracted from each simulated configuration:

1. Stiffness as the secant to 80% of the maximum force,
2. Strength as the maximum force recorded,
3. Displacement u_{50} at the point the force drops to 50% of its maximum value,
4. Toughness as the integral of F - u up u_{50} , and
5. Displacement u_{slip} at the point the magnitude of the frictional dissipation becomes greater than the strain energy ($ALLFD > ALLSE$).

3. Results

Results for computations for three exemplar assemblies are shown first: (i) the [3.4.6.4]-B system with a single tile type, Fig. 3(a), (ii) the [4.8²]-A(+) system with two different tiles, Fig. 4(a), and (iii) the [4.6.12]-A(+) system composed of three different tiles, Fig. 5(a). The computed force (F) - displacement (u) records for the indenter are shown in Figs 3(b), 4(b), 5(b), while the corresponding records of system energies $ALLWK$, $ALLSE$, $ALLFD$ are shown in Figs 3(c), 4(c), 5(c).

The F - u curves (Figs 3(b), 4(b), 5(b)) overall possess the skewed parabola shape with a gradual load decrease past the maximum load, similar to what has been documented in other investigations on TIM systems [20, 21, 22, 23]. Stiffness, strength, toughness, the rate of force drop post the load maximum, and the slip onset vary distinctly between assembly architectures. Initially, the F - u curves are smooth and deformation is by tilting of unit blocks and their elastic deformation. As deformation progresses, local slip events become apparent in the F - u curve as intermittent load drops.

The three examples depicted represent conditions where the onset of slip dominance is significantly different. The contribution of slip to the deformation response can be assessed from the evolution of the systems energies during loading, Figs 3(c), 4(c), 5(c). For the [3.4.6.4]-B case, slip is a strongly dominant factor. Friction dissipation is of equal magnitude as the strain energy already during early stages of loading, and slip becomes dominant past the maximum load at $u = 7.58$ mm. For the [4.8²]-B configuration and the [4.6.12]-A(+) case, the strain energy is much larger than the frictional dissipation over much of the load history. The slip onset condition is delayed to $u_{slip}=21.05$ mm for the [4.8²]-B case and to $u_{slip}=20.6$ mm [4.6.12]-A(+)

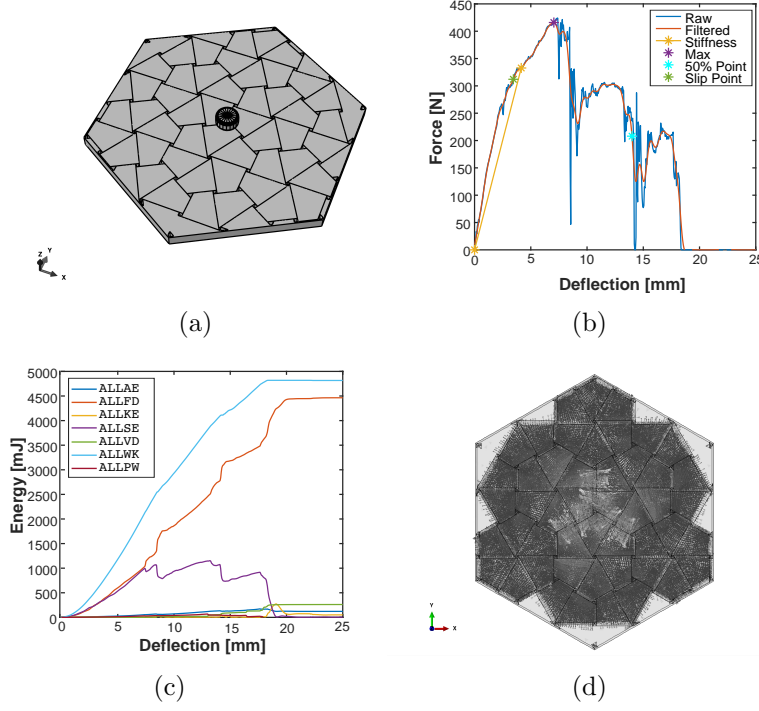


Figure 3: (a) The [3.4.6.4]-B TIM system constructed with one tile type, (b) System energies, (c) Force-deflection response, (d) Vector plot of compressive principal stresses σ_{p3} at the maximum load $\sigma_{p3} = [-28, +1]$ MPa.

case, far into the deformation histories. Slip alone is not the sole determining factor for the strength of a system. While the [3.4.6.4]-B with the largest slip contribution also possesses the lowest strength $F_{max} = 415.9$ N, the two other systems possess distinctly different strength despite similarly delayed slip: F_{max} for [4.8²]-B is 872.7 N and for [4.6.12]-A(+) it is 1249.0 N. Past the maximum load, failure is gradual at least until the latest stages of the deformation history. For the [3.4.6.4]-B assembly, strong local intermittent load drops are associate with slip events and load carrying capacity is lost early, ($u_{50} = 14.0$ mm). For the other two assemblies slip events are less pronounced in the F - u data, and u_{50} values are significantly larger: $u_{50} = 15.6$ mm for [4.8²]-B and 17.3 mm for [4.6.12]-A(+). As a consequence, toughness values are also significantly different. The toughness is the least for [3.4.6.4]-B, followed by [4.8²]-B and [4.6.12]-A(+).

In TIM systems, load transfer is dominated by compressive loads in build-

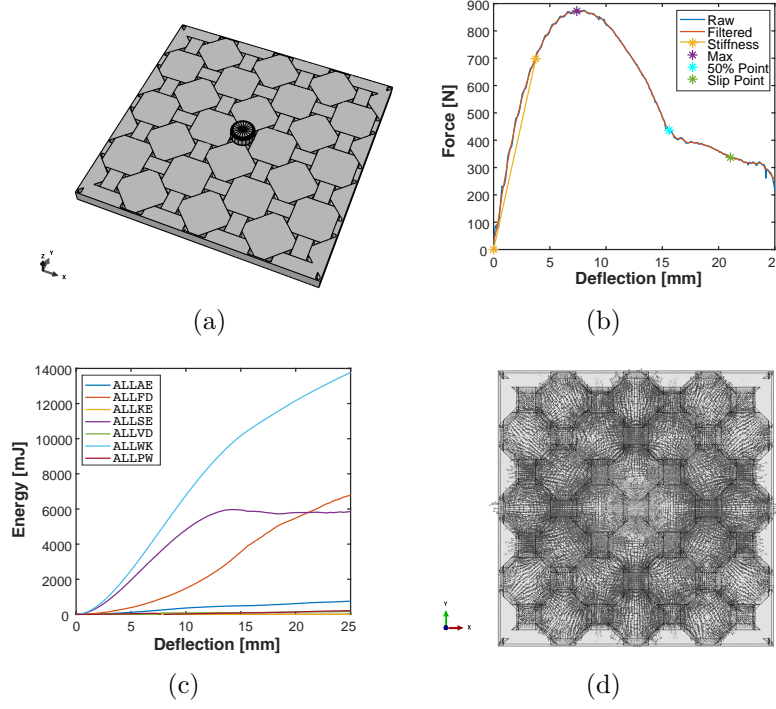


Figure 4: (a) The $[4.8^2]$ -B TIM system constructed with two tile types, (b) System energies (c) Force-deflection response, Vector plot of compressive principal stresses σ_{p3} at the maximum load with $\sigma_{p3} = [-52, +2]$ MPa.

ing blocks balanced by tensile loads in the bounding frame. The computed load transfer patterns in the assemblies are depicted as vector plots of the compressive principal stress σ_{p3} at the state of maximum load. In the assembly [3.4.6.4]-B the distribution of σ_{p3} is found to be rather homogeneous throughout and the entire assembly perimeter transfers load to the bounding frame, Fig. 3(d). For the assembly $[4.8^2]$ -B it is found that σ_{p3} is less in the larger tiles than it is in the smaller ones and a distinct load transfer pattern is seen, Fig. 4(d). Now loads are transferred to the frame only along a subset of faces to the bounding frame but both types of tiles contribute. The finding of load transfer being dominant via the smallest building blocks is also present in the results for the [4.6.12]-A(+) assembly, Fig. 5(d). In this case load transfer to the frame is found to occur predominantly via the faces of the smallest building blocks.

Subsequently, the characteristics of all computed configurations are con-

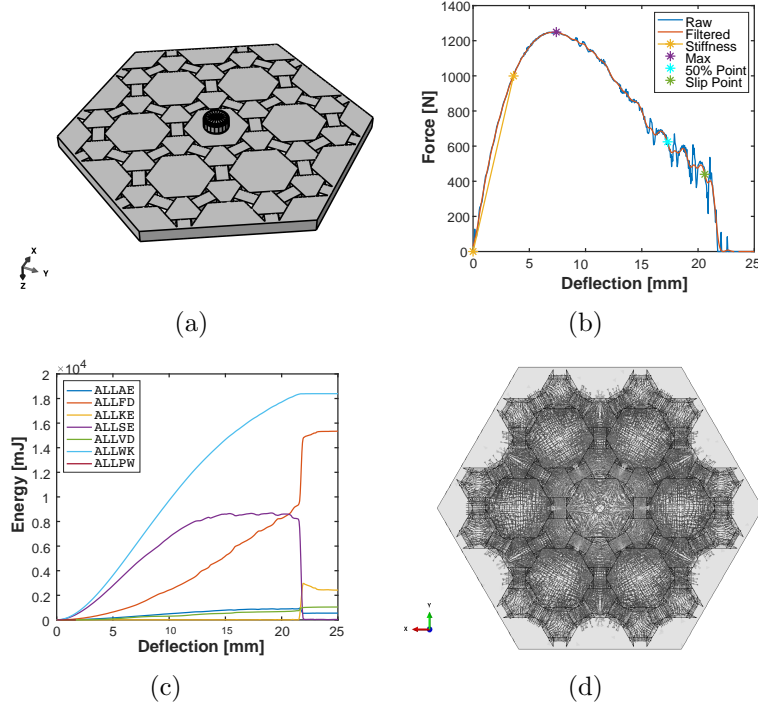


Figure 5: (a) The [4.6.12]-A(+) TIM system constructed with three tile types, (b) System energies, (c) Force-deflection response, (d) Vector plot of compressive principal stresses σ_{p3} at the maximum load with $\sigma_{p3} = [-120, +1]$ MPa.

254 sidered in the form of cross-property relationships. Strength and stiffness
 255 were linearly correlated to a high degree, Fig. 6(a). Stiffness and toughness,
 256 Fig. 6(b), ($R^2=0.65$) as well as strength and toughness, Fig. 6(c), ($R^2=0.80$)
 257 are also linearly correlated, but at a somewhat smaller R^2 value. From the
 258 results Figs 3, 4 and 5 it could be inferred that the prevalence of slip would
 259 be a good predictor of TIM properties. However, this was found to be only
 260 partially the case. Strength is related to u_{slip} but the correlation is weak,
 261 Fig. 6(d) ($R^2=0.64$). The relationship between stiffness and u_{slip} is even
 262 weaker at $R^2 = 0.43$.

263 4. Discussion

264 The TIM plate systems introduced in this study exhibit attractive prop-
 265 erties in terms of their failure. Conventional plate theory cannot be used to

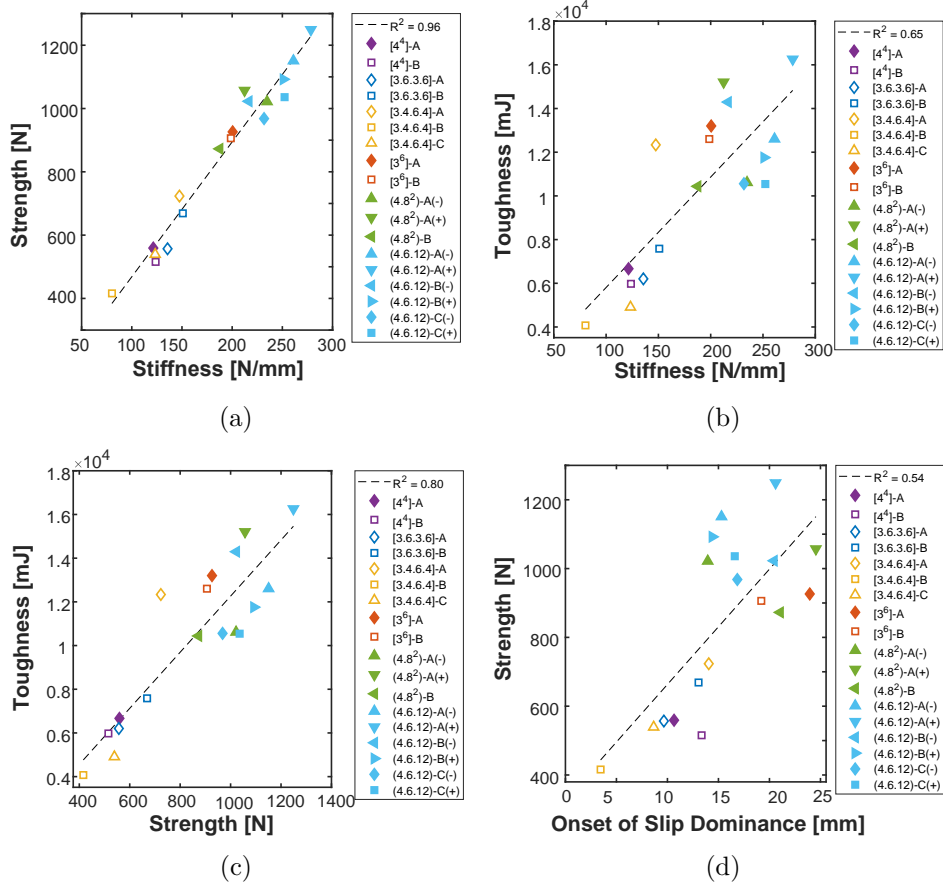


Figure 6: Cross property relationships: (a) Strength and stiffness, (b) Toughness and stiffness (c) Toughness and strength (d) Stiffness and onset of slip dominance.

266 describe the systems under consideration, despite the fact that the mechani-
 267 cal function (to carry transverse loads) is the same for monolithic plates and
 268 the TIM systems presented here. In the TIM plate systems gradual decrease
 269 in load past the maximum load is realized even if the material used to make
 270 the building blocks would be considered as brittle itself. Such a response is
 271 found across all system architectures considered.

272 The overall transverse force-deflection response of TIM systems can be
 273 explained by the formation of multiple force chains in the granular-like as-
 274 sembly. Such force chains are distinctly visible in Fig. 5(d), i.e. the strongest
 275 TIM system here, but to a lesser extent in Fig. 3(d), i.e. the weakest TIM
 276 system here. In the TIM systems, force chains extend from the top plate

face at the location at which the load is applied to the opposing bottom plate face and the plate support. In the mechanics of granular materials, it is common practice to ascribe truss and beam mechanics characteristics (such as buckling) to describe the force chain response under load [49]. As the plate deflection increases so do the angles between the force chains and the plate reference plane. Such a process is similar to what happens in a Mises-truss. In [45] a comprehensive model for this approach was demonstrated for the [4⁴]-A tiling. In the conventional Mises truss, the transverse force (F) is related to the initial and current angle of inclination of the trusses, θ_0 and θ , respectively, as:

$$F = \frac{2EA}{L} \left[1 - \frac{\cos \theta_0}{\cos(\theta_0 - \theta)} \right] \sin(\theta_0 - \theta) \quad (1)$$

with EA/L stiffness of the individual trusses, with E the modulus of the truss, A the cross section and L the length. Furthermore, θ_0 the inclination of the trusses in the initial configuration and θ the rotation of the trusses during deformation. The maximum force value, F_{max} , i.e. the strength of the Mises truss is:

$$F_{max} = \frac{2EA}{L} \left[1 - \sqrt[3]{\cos^2 \theta_0} \right]^{3/2} \quad (2)$$

In the application of the Mises truss model to the TIM plates, the following geometric correlations applies $\tan \theta_0 \approx H_0/L_0$. Also, $F > 0$ as the block to block interactions do not carry tension. The stiffness of the trusses (EA/L) is replaced by a stiffness K_0 which represents the stiffness of the force chain. In granular systems, the stiffness of the force chain K_0 is related to a mechanical stiffness K_c (representing the the contact interaction) and a geometrical stiffness K_g (representing the contact force and particle shape), [50]. In a model in which slip is absent and $\tan \theta \approx (H_0 - u)/L_0$. In a more realistic case, θ is modified to account for slip as $\theta(1 + \gamma)$, where γ is a slip coefficient. Then, the Mises truss model for the deflection of TIM plate is given as:

$$F = (K_c + K_g) \left\{ 1 - \frac{\cos \theta_0}{\cos[\theta_0 - \theta(1 + \gamma)]} \right\} \sin[\theta_0 - \theta(1 + \gamma)] \quad (3)$$

whereas the TIM plate strength is

$$F_{max} = (K_c + K_g) \left[1 - \sqrt[3]{\cos^2 \theta_0} \right]^{3/2} \quad (4)$$

304 Consequently, the stiffness (K) of the TIM plate is

$$K = \frac{F_{max}}{H_0/2} \quad (5)$$

305 The toughness (W) is

$$W = \frac{1}{2}F_{max}2H_0 \quad (6)$$

306 where the factor 2 account for the presence multiple sequential force
 307 chains in the system [45]. From the Mises model, the observation of a linear
 308 dependence of strength on stiffness, 6(a), of toughness on stiffness, 6(b), and
 309 of toughness on strength, ??, is consistent.

310 It is of interest to relate the system mechanical characteristics to the ar-
 311 chitectural aspects in order to find predictors of system performance. As
 312 strength is well correlated with both stiffness and toughness, a predictor
 313 for strength is also capable of predicting stiffness and toughness. To start,
 314 strength was correlated against measures of the degree of segmentation.
 315 First, the number of tiles in an assembly is considered, Table 1. For the
 316 relationship between number of tiles and strength the coefficient of determi-
 317 nation $R^2 = 0.02$. Next, strength was correlated against the degree of seg-
 318 mentation in the assembly. One measure of the degree of segmentation is the
 319 total contact area between all segmented bodies in the assembly. The total
 320 contact area between all segmented bodies in the assembly is computed in the
 321 assembly's initial position before any displacement had occurred. Strength
 322 and total contact area between all segmented bodies in the assembly are
 323 well correlated, Fig. 7(a) ($R^2 = 0.77$). Smaller values of total contact area
 324 lead to higher strength. This suggests that the less segmented a structure
 325 is, the greater its strength will be. This argument would intuitively agree
 326 with the fact that a monolithic plate is generally stronger than its segmented
 327 counterparts. A second measure of the degree of segmentation is the number
 328 of contact interfaces in the assembly, defined as a state of contact between
 329 any two bodies. Strength and the number of contact interfaces are less sig-
 330 nificantly related, Fig. 7(b) ($R^2 = 0.61$), but an increase in the number of
 331 contact interfaces is correlated to an increase in strength suggesting that the
 332 more segmented a structure is, the greater its strength will be. The correla-
 333 tions between strength and the two measures of segmentation are in obvious
 334 disagreement. Clearly, to determine the degree of segmentation alone is in-
 335 sufficient in predicting the properties of the TIM systems under consideration
 336 here.

337 The present data suggests that TIM behavior must be dependent on how
 338 the system is segmented rather than how much it is segmented. The assem-
 339 blies having a larger number of contact interfaces did so by having building
 340 blocks with a greater number of sides. It is possible to increase the number of
 341 contact interfaces by increasing the number of building blocks, but the TIM
 342 systems in this study all had approximately the same number of building
 343 blocks. Therefore, the increase in strength seen with the increase in con-
 344 tact interfaces might be attributed to the presence of larger building blocks,
 345 rather than to the increase in contact interfaces. This might describe the
 346 gap in strength values that is seen between the weakest configurations (all
 347 based on tessellations with a single four-sided tile) and the other configura-
 348 tions which also include larger tiles with a larger number of sides, Fig. 7(b).
 349 To further investigate the dependence of the mechanical behavior on sys-
 350 tem architecture, strength is correlated against the area of the largest tile
 351 in the tessellation from which each TIM system was constructed, Fig. 8(a).
 352 Strength is found as positively correlated with the largest tile area in the
 353 assembly ($R^2 = 0.52$). This finding does support the previous conjecture
 354 that TIM systems with larger blocks would be stronger, but with a coeffi-
 355 cient of determination $R^2 = 0.52$ it is not a strong correlation. Given that
 356 the bounded tilings in this study all have approximately the same number
 357 of tiles and about the same total area, if there are larger tiles in a tiling, it
 358 must also possess some smaller tiles. Thus, strength is correlated against the
 359 area of the smallest tile in the tessellation from which each TIM system was
 360 constructed, Fig. 8(b). This relationship possesses a coefficient of determi-
 361 nation $R^2 = 0.73$ and suggests that the smallest tile size is a better predictor
 362 of strength than the largest tile size.

363 In terms of the Mises truss model for the deformation of TIM plate defor-
 364 mation, the type of segmentation affects the geometric stiffness K_g such that
 365 assemblies with larger tiles as part of the assembly, 5, possess larger values
 366 of K_g than those with all equal sized tiles, 3. In systems with high K_g the
 367 force chain character is also more distinct than in systems of smaller K_g .
 368 Larger stiffness values will lead to higher values of contact pressure and thus
 369 a reduced value of slip, i.e. a larger value of the slip factor γ . The findings on
 370 architecture-property relationships suggest that the strongest TIM systems
 371 are the ones with the least total contact area, the greatest number of contact
 372 interfaces, and the largest (sic smallest) tiles as part of the assembly. This
 373 combination of characteristics leads to the conclusion that TIM system con-
 374 figurations having architectures that constrict load transfer into well defined

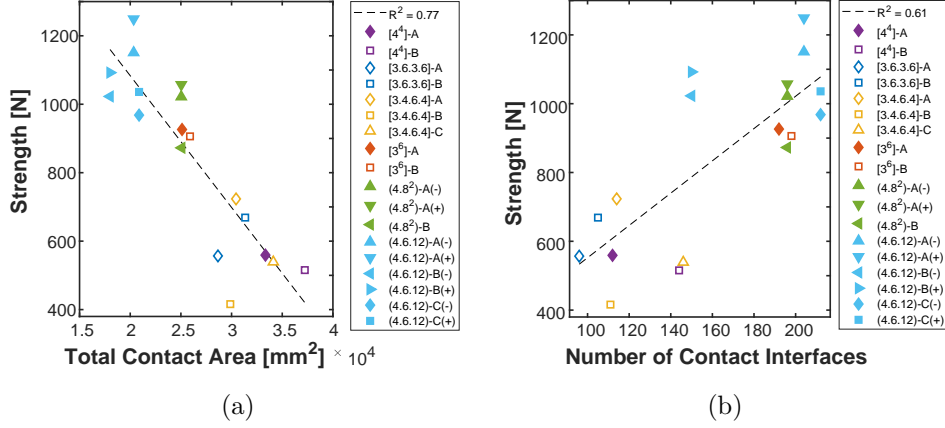


Figure 7: Mechanical properties and global measures of segmentation: (a) Strength vs total contact area between segmented bodies; (b) Strength vs number of contact interfaces between segmented bodies.

force chains possess the greatest strength. These increasing degrees in the concentration of force chains are well represented in the results of the computations for the TIM configurations based on the [3.4.6.4]-B, [4.8²]-B, and [4.6.12]-A tilings, Figs 3(d), 4(d), 5(d). A more distinctly developed force chain network is thereby not related only to the presence of smaller tiles in the assembly but also to the geometry of the tessellation as the force chain network structure develops within a specific assembly.

The present results were confined by two constraints: assemblies are planar and the interlocking geometry is based on planar tile faces. Neither constraint is seen as a limitation in the application of present results. The geometric arguments on tessellations and the resulting assemblies overall can certainly be extended to curved systems made of topologically interlocked building blocks which have recently been demonstrated in the context of digital design and manufacturing approaches [34, 51, 52]. As it has been demonstrated that osteomorphic shaped interlocking [53, 54] and multiscale interlocking [55] provide similar or improved mechanical response as planar type interlocking, it can be argued that the present results will be applicable to such systems as well.

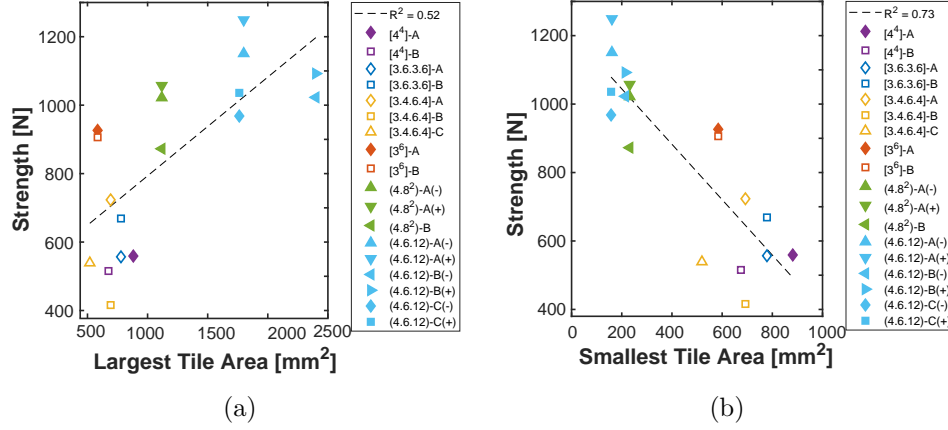


Figure 8: Mechanical properties and maximum measures of segmentation: (a) Strength vs area of the largest tile in the base tiling; (b) Strength vs area of the smallest tile in the base tiling.

5. Conclusion

TIM systems were constructed for 18 configurations based on six unique tilings and their response under transversely applied displacement load is investigated. It was found that the load responses of all configurations were generally consistent with the typical skewed parabola that has been recorded in other TIM systems and can well be described by an application of the Mises truss model to the internal force chain structure. The attractive positive correlations of toughness-stiffness and toughness-strength were realized for all configurations. There exists significant variance in the performance of the TIM systems in this study. It was generally observed that the triple-tile (4.6.12) configurations were the strongest, followed but the double-tile (4.8²) configurations, the single hexagon tile [3⁶] configurations, and then all the single four-sided tile configurations. The stiffest, strongest, and toughest configurations tended to have the least total contact area between segmented bodies, the greatest number of contact interfaces, and the smallest tiles. It is postulated that this combination of features leads to more confined force chains of the internal load transfer. The findings of this study allow for an expansion of the material space. When considering a segmented material system, a greater range of ductility is available as compared to homogeneous materials. The tessellation pattern can be chosen to achieve the desired ductility. These methods can be used to design advantageous material systems.

414 that are ductile as a system while maintaining high strength within the in-
415 dividual components.

416

417 **Acknowledgment:** This work supported by the National Science Founda-
418 tion under Grant No. 1662177.

419 Appendix A. TIM Assemblies

420 Figures A.9 to Fig. A.14 depict the TIM systems under consideration as
 421 3D model geometries (i.e. using visualization capabilities in the graphical
 422 user interface of the ABAQUS/CAE code). The rigid frames colored blue
 423 and the individual elastic building blocks in yellow. The centrally located
 424 cylinder represents the indenter through which the mechanical load is applied.

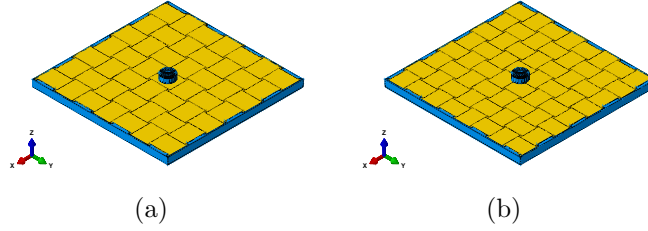


Figure A.9: Assembly configurations: (a) $[4^4]$ -A, (b) $[4^4]$ -B.

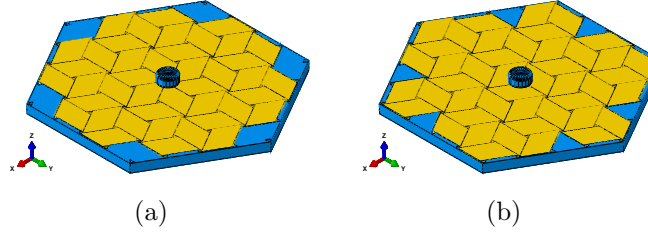


Figure A.10: Assembly configurations: (a) $[3.6.3.6]$ -A, (b) $[3.6.3.6]$ -B.

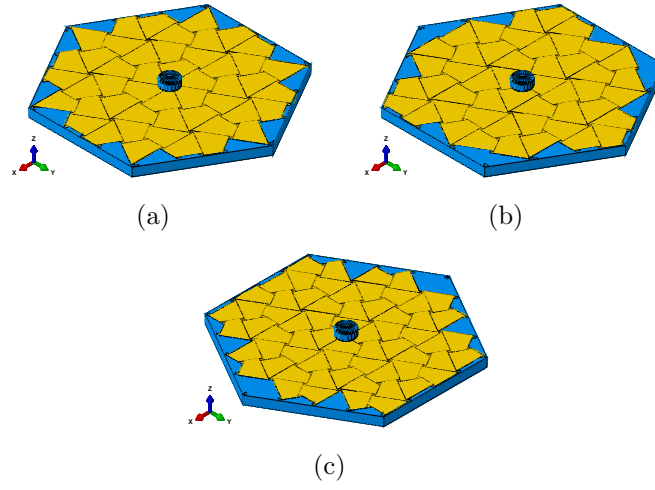


Figure A.11: Assembly configurations: (a) [3.4.6.4]-A, (b) [3.4.6.4]-B, (c) [3.4.6.4]-C.

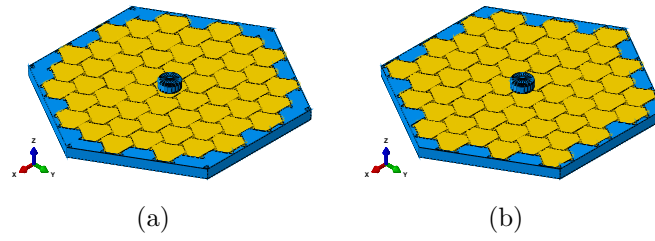


Figure A.12: Assembly configurations: (a) [3⁶]-A, (b) [3⁶]-B.

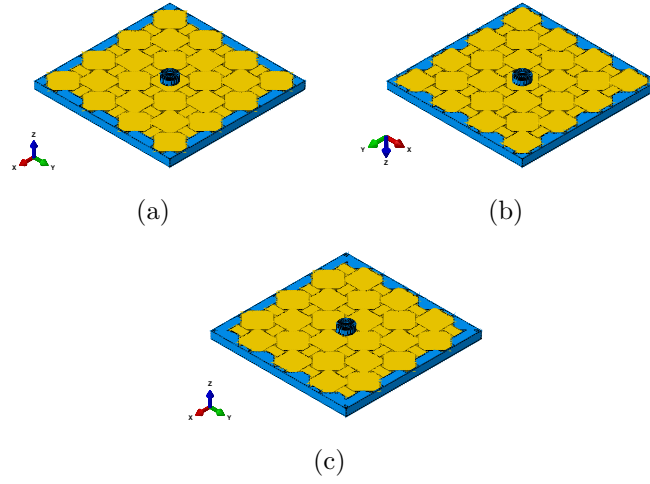


Figure A.13: Assembly configurations: (a) (4.8^2) -A(-), (b) (4.8^2) -A(+), (c) (4.8^2) -B.

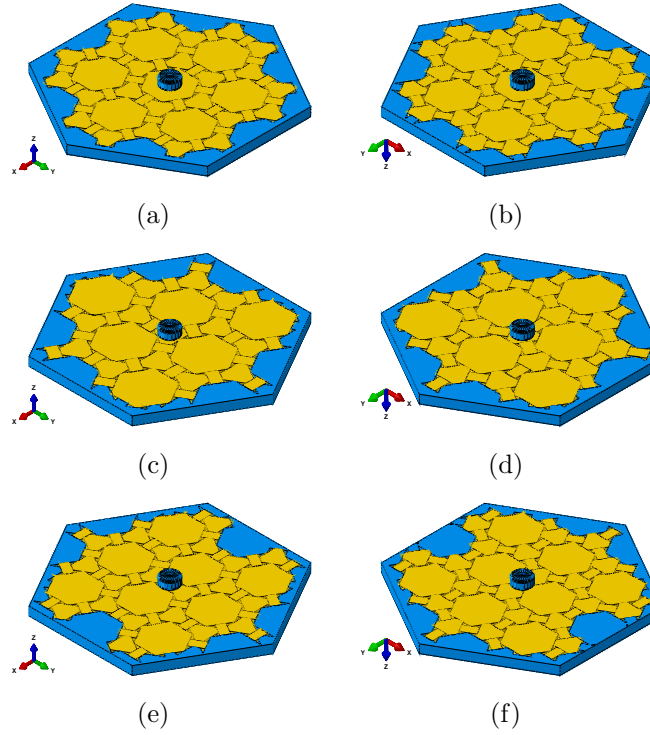


Figure A.14: Assembly configurations: (a) $(4.6.12)$ -A(-), (b) $(4.6.12)$ -A(+), (c) $(4.6.12)$ -B(-), (d) $(4.6.12)$ -B(+), (e) $(4.6.12)$ -C(-), (f) $(4.6.12)$ -C(+).

425 Appendix B. Analysis Approach

426 All model configurations are analyzed with finite element method. The
427 finite element method used is an implementation of the central difference
428 integration rule together with the use of diagonal element mass matrices
429 (ABAQUS). Only the quasi-static response of the system is of concern. In
430 the computations a quasi-static response is obtained through the use of the
431 mass scaling concept. Both a damping term related to the volumetric strain
432 rate and the square of the volumetric strain rate are considered.

433 The frame was made to be undeformable and fixed in space. The elastic
434 modulus of the unit elements was assigned to be $E = 1.83$ GPa, the Poisson
435 ratio $\nu = 0.35$. These properties are motivated by a 3D printing manu-
436 facturing approach for the physical realization of interlocked assemblies [14].
437 Contact was defined between all bodies with a stiff linear pressure-overclosure
438 relationship and a coefficient of friction of $\mu = 0.2$. A density $\rho = 0.95$ g/cm³
439 was considered and mass scaling by a factor of 100 was employed to reduce
440 computation time. 8-node reduced integration hexahedral elements (C3D8R)
441 were used to mesh the blocks, while solid 4-node tetrahedral elements (C3D4)
442 were used for the rigid frame. Enhanced hourglass control was used on the
443 hexahedral elements to reduce an observed tendency for hourglassing with
444 default hourglass control. The computed reaction forces on the indenter were
445 filtered using a second order Butterworth filter with a cutoff frequency of 50
446 Hz.

447 Several steps were undertaken to ensure the accuracy of the model com-
448 putation. In all computations the quasi-static mechanical response ensured
449 as the external work ALLWK is the sum of strain energy ALLSE and fric-
450 tion dissipation ALLFD. All other contributions (penalty work in the contact
451 ALLPW, viscous dissipation ALLVD, artificial energies ALLAE and kinetic energy
452 ALLKE) are negligible, at least up to conditions where slip starts to dominate
453 and $ALLSE < ALLFD$. Mesh convergence was evaluated by comparing force-
454 deflection data for each of the models for mesh seed size over a range from
455 $0.15 H_0$ to $0.21 H_0$ in increments of $0.01 H_0$. It was found that convergent re-
456 sults for the computed force-deflection behavior were obtained for almost all
457 cases if the mesh seed size is $0.16 H_0$. The exception to that finding were the
458 [4⁴]-A and [4⁴]-B configurations. These cases were susceptible to a perfect
459 alignment of meshes across contacts which tends to result in a nontraditional
460 hourglassing across contact interfaces. Such cross-contact hourglassing would
461 create a local interlocking feature between the blocks and prevent sliding. A

seed size of $0.17H_0$ was used for the $[4^4]$ -A and $[4^4]$ -B configurations to avoid
the mesh alignment issues.

References

- [1] P. G. Lowe, Basic principles of plate theory, Springer Science & Business Media, 2012.
- [2] J.-G. Gallon, Machines et inventions approuvées par l'Academie Royale des Sciences depuis son établissement jusqu'à présent; avec leur description, volume 7, chez Gabriel Martin, Jean-Baptiste Coignard, fils, Hippolyte-Louis Guerin, 1777.
- [3] M. Glickman, The G-block system of vertically interlocking paving, in: Second International Conference on Concrete Block Paving, Delft, Netherlands, 1984.
- [4] M. Rippmann, P. Block, Rethinking structural masonry: unreinforced, stone-cut shells, Proceedings of the Institution of Civil Engineers-Construction Materials 166 (2013) 378–389.
- [5] G. Fallacara, M. Barberio, An unfinished manifesto for stereotomy 2.0, Nexus Network Journal 20 (2018) 519–543.
- [6] I. M. Vella, T. Kotnik, Geometric Versatility of Abeille Vault, Proceedings of the 34th International Conference on Education and Research in Computer Aided Architectural Design in Europe 2 (2016) 391–397.
- [7] O. Tessmann, Topological interlocking assemblies, in: Physical Digitality—Proceedings of the 30th International Conference on Education and Research in Computer Aided Architectural Design in Europe, Prague, Czech Republic, Sept, 2012, pp. 12–14.
- [8] O. Tessmann, A. Rossi, Geometry as interface: Parametric and combinatorial topological interlocking assemblies, Journal of Applied Mechanics 86 (2019).
- [9] A. V. Dyskin, Y. Estrin, E. Pasternak, H. C. Khor, A. J. Kanel-Belov, The principle of topological interlocking in extraterrestrial construction, Acta Astronautica 57 (2005) 10–21.
- [10] A. V. Dyskin, Y. Estrin, A. J. Kanel-Belov, E. Pasternak, Toughening by fragmentation—how topology helps, Advanced Engineering Materials 3 (2001) 885–888.

- 495 [11] A. Dyskin, Y. Estrin, A. Kanel-Belov, E. Pasternak, A new concept
496 in design of materials and structures: assemblies of interlocked
497 tetrahedron-shaped elements, *Scripta Materialia* 44 (2001) 2689–2694.
498 doi:10.1016/S1359-6462(01)00968-X.
- 499 [12] F. Barthelat, Architected materials in engineering and biology: fabri-
500 cation, structure, mechanics and performance, *International Materials*
501 *Reviews* 60 (2015) 413–430.
- 502 [13] H.-C. Ries, M. V. Carlesso, C. Eigenbrod, S. Kroll, K. Rezwan, On
503 the performance of porous sound absorbent ceramic lining in a combus-
504 tion chamber test rig, in: *ASME Turbo Expo 2013: Turbine Technical*
505 *Conference and Exposition*, American Society of Mechanical Engineers
506 Digital Collection, 2013.
- 507 [14] T. Siegmund, F. Barthelat, R. Cipra, E. Habtour, J. Riddick, Manu-
508 facture and mechanics of topologically interlocked material assemblies,
509 *Applied Mechanics Reviews* 68 (2016) 040803.
- 510 [15] Z. Wang, P. Song, F. Isvoranu, M. Pauly, Design and structural opti-
511 mization of topological interlocking assemblies, *ACM Transactions on*
512 *Graphics (TOG)* 38 (2019) 1–13.
- 513 [16] Y. Estrin, A. V. Dyskin, E. Pasternak, H. C. Khor, A. J. Kanel-Belov,
514 Topological interlocking of protective tiles for the space shuttle, *Philo-*
515 *sophical Magazine Letters* 83 (2003) 351–355.
- 516 [17] M. F. Ashby, Hybrids to fill holes in material property space, *Philo-*
517 *sophical Magazine* 85 (2005) 3235–3257.
- 518 [18] M. F. Ashby, Hybrid materials to expand the boundaries of material-
519 property space, *Journal of the American Ceramic Society* 94 (2011)
520 s3–s14.
- 521 [19] Y. Estrin, A. V. Dyskin, E. Pasternak, Topological interlocking as a
522 material design concept, *Materials Science and Engineering C* 31 (2011)
523 1189–1194.
- 524 [20] A. Mather, R. Cipra, T. Siegmund, Structural integrity during remanu-
525 facture of a topologically interlocked material, *International Journal of*
526 *Structural Integrity* 3 (2012) 61–78.

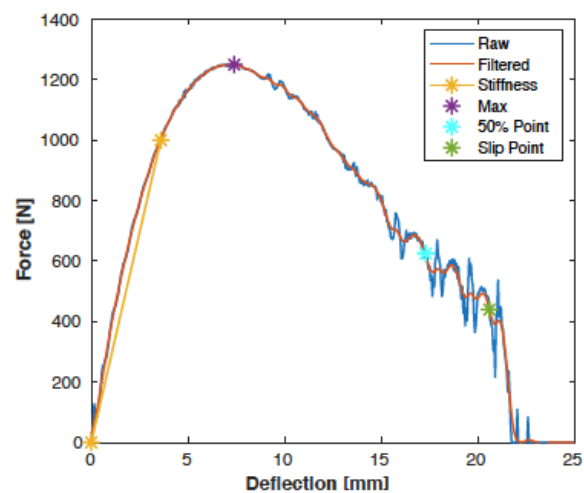
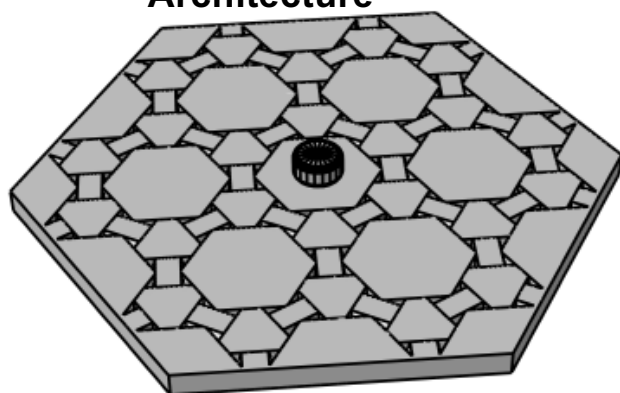
- 527 [21] S. M. M. Valashani, F. Barthelat, A laser-engraved glass duplicating the
528 structure, mechanics and performance of natural nacre, *Bioinspiration*
529 & *Biomimetics* 10 (2015) 026005.
- 530 [22] A. V. Dyskin, Y. Estrin, E. Pasternak, H. C. Khor, A. J. Kanel-Belov,
531 Fracture resistant structures based on topological interlocking with non-
532 planar contacts, *Advanced Engineering Materials* 5 (2003) 116–119.
- 533 [23] M. Mirkhalaf, T. Zhou, F. Barthelat, Simultaneous improvements of
534 strength and toughness in topologically interlocked ceramics, *Proceed-*
535 *ings of the National Academy of Sciences* 115 (2018) 9128–9133.
- 536 [24] Y. Feng, T. Siegmund, E. Habtour, J. Riddick, Impact mechanics of
537 topologically interlocked material assemblies, *International Journal of*
538 *Impact Engineering* 75 (2015) 140–149.
- 539 [25] A. R. Javan, H. Seifi, S. Xu, Y. M. Xie, Design of a new type of interlock-
540 ing brick and evaluation of its dynamic performance, in: *Proceedings*
541 *of IASS Annual Symposia*, volume 2016, International Association for
542 *Shell and Spatial Structures (IASS)*, 2016, pp. 1–8.
- 543 [26] A. R. Javan, H. Seifi, S. Xu, D. Ruan, Y. Xie, The impact behaviour of
544 plate-like assemblies made of new interlocking bricks: An experimental
545 study, *Materials & Design* 134 (2017) 361–373.
- 546 [27] A. Rezaee Javan, H. Seifi, S. Xu, X. Lin, Y. M. Xie, Impact behaviour
547 of plate-like assemblies made of new and existing interlocking bricks:
548 A comparative study, *International Journal of Impact Engineering* 116
549 (2018) 79–93.
- 550 [28] S. Khandelwal, T. Siegmund, R. J. Cipra, J. S. Bolton, Adaptive me-
551 chanical properties of topologically interlocking material systems, *Smart*
552 *Materials and Structures* 24 (2015) 045037.
- 553 [29] A. Molotnikov, R. Gerbrand, Y. Qi, G. P. Simon, Y. Estrin, Design
554 of responsive materials using topologically interlocked elements, *Smart*
555 *Materials and Structures* 24 (2015) 025034.
- 556 [30] A. V. Dyskin, Y. Estrin, A. J. Kanel-Belov, E. Pasternak, Topological
557 interlocking of platonic solids: A way to new materials and structures,
558 *Philosophical Magazine Letters* 83 (2003) 197–203.

- 559 [31] M. Weizmann, O. Amir, Y. J. Grobman, Topological interlocking in
560 architecture: A new design method and computational tool for designing
561 building floors, *International Journal of Architectural Computing* 15
562 (2017) 107–118.
- 563 [32] M. Weizmann, O. Amir, Y. J. Grobman, Topological interlocking in
564 buildings: A case for the design and construction of floors, *Automation
565 in Construction* 72 (2016) 18–25.
- 566 [33] M. Weizmann, O. Amir, Y. Grobman, Topological interlocking in ar-
567 chitectural design, *CAADRIA 2015 - 20th International Conference on
568 Computer-Aided Architectural Design Research in Asia: Emerging Ex-
569 periences in the Past, Present and Future of Digital Architecture* (2015).
- 570 [34] A. Bejarano, C. Hoffmann, A generalized framework for designing topo-
571 logical interlocking configurations, *International Journal of Architec-
572 tural Computing* 17 (2019) 53–73.
- 573 [35] M. Piekarski, New concepts for application of topological interlocking
574 in architecture, in: *Shape, Form and Geometry -Applications*, eCAADe
575 36, volume 2, 2018, pp. 467–478.
- 576 [36] M. Rippmann, P. Block, Computational tessellation of freeform, cut-
577 stone vaults, *Nexus Network Journal* 20 (2018) 545–566.
- 578 [37] B. Grünbaum, G. C. Shephard, *Tilings & Patterns*, second ed., Dover
579 Publications, Inc., Mineola, New York, 2016.
- 580 [38] A. J. Kanel-Belov, A. V. Dyskin, Y. Estrin, E. Pasternak, I. A. Ivanov-
581 Pogodaev, Interlocking of convex polyhedra: Towards a geometric the-
582 ory of fragmented solids, *Moscow Mathematical Journal* 10 (2010) 337–
583 342.
- 584 [39] M. Brocato, L. Mondardini, A new type of stone dome based on Abeille’s
585 bond, *International Journal of Solids and Structures* 49 (2012) 1786–
586 1801.
- 587 [40] M. Brocato, A continuum model of interlocking structural systems,
588 *Atti della Accademia Nazionale dei Lincei, Classe di Scienze Fisiche,
589 Matematiche e Naturali, Rendiconti Lincei Matematica e Applicazioni*
590 29 (2018) 63–83.

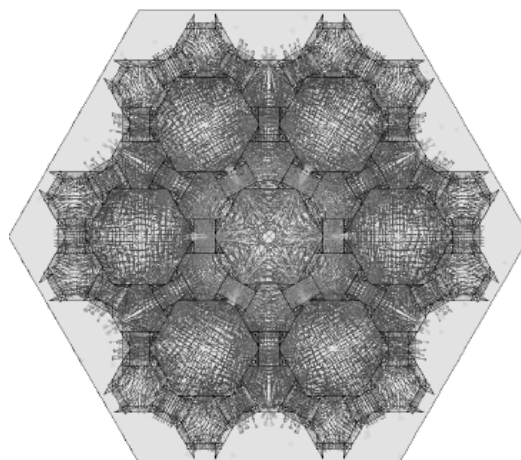
- 591 [41] M. Fantin, T. Ciblac, M. Brocato, Resistance of flat vaults taking their
592 stereotomy into account, *Journal of Mechanics of Materials and Structures* 13 (2019) 657–677.
593
- 594 [42] A. Pfeiffer, F. Lesellier, M. Tournier, Topological interlocking assemblies
595 experiment, in: *Design Modelling Symposium Berlin*, Springer, 2019,
596 pp. 336–349.
- 597 [43] S. Khandelwal, T. Siegmund, R. J. Cipra, J. S. Bolton, Scaling of the
598 Elastic Behavior of Two-Dimensional Topologically Interlocked Materi-
599 als Under Transverse Loading, *Journal of Applied Mechanics* 81 (2013)
600 031011.
- 601 [44] S. Khandelwal, T. Siegmund, R. J. Cipra, J. S. Bolton, Transverse load-
602 ing of cellular topologically interlocked materials, *International Journal*
603 *of Solids and Structures* 49 (2012) 2394–2403.
- 604 [45] M. Short, T. Siegmund, Scaling, growth, and size effects on the mechan-
605 ical behavior of a topologically interlocking material based on tetrahedra
606 elements, *Journal of Applied Mechanics* 86 (2019) 111007.
- 607 [46] A. Dyskin, Y. Estrin, E. Pasternak, Topological interlocking materials,
608 in: *Architected Materials in Nature and Engineering*, Springer, 2019,
609 pp. 23–49.
- 610 [47] M. F. Ashby, Material and process selection charts, *The CES EduPack*
611 *Resource Booklet* 2 (2010) 42.
- 612 [48] A. Williams, Abaqus python code for the simulation of topologically
613 interlocked material systems based on archimedean and laves tilings, in:
614 *Purdue University Research Repository*, 2020. doi:10.4231/JBKY-JH21.
- 615 [49] A. Tordesillas, Force chain buckling, unjamming transitions and shear
616 banding in dense granular assemblies, *Philosophical Magazine* 87 (2007)
617 4987–5016.
- 618 [50] M. R. Kuhn, C. S. Chang, Stability, bifurcation, and softening in discrete
619 systems: a conceptual approach for granular materials, *International*
620 *Journal of Solids and Structures* 43 (2006) 6026–6051.

- 621 [51] G. Fallacara, Digital stereotomy and topological transformations: rea-
 622 soning about shape building, in: Proceedings of the second international
 623 congress on construction history, volume 1, 2006, pp. 1075–1092.
- 624 [52] P. Block, M. Rippmann, T. Van Mele, D. Escobedo, The armadillo
 625 vault: Balancing computation and traditional craft, Fabricate (2017)
 626 286–293.
- 627 [53] A. Molotnikov, Y. Estrin, A. Dyskin, E. Pasternak, A. Kanel-Belov,
 628 Percolation mechanism of failure of a planar assembly of interlocked
 629 osteomorphic elements, Engineering fracture mechanics 74 (2007) 1222–
 630 1232.
- 631 [54] F. Oikonomopoulou, Experimental and numerical investigation of an
 632 interlocking system out of osteomorphic cast glass components, A+
 633 BE— Architecture and the Built Environment 9 (2019) 247–296.
- 634 [55] L. Djumas, G. P. Simon, Y. Estrin, A. Molotnikov, Deformation me-
 635 chanics of non-planar topologically interlocked assemblies with struc-
 636 tural hierarchy and varying geometry, Scientific reports 7 (2017) 1–11.

Plates with Interlocked Tile Architecture



Mechanical Response & Load Transfer Patterns



Architecture-Property Relationships

